Peer reviewed version

Link to published version (if available):
10.1021/acs.jpcb.6b09916

Link to publication record on the Bristol Research Portal
PDF-document

University of Bristol – Bristol Research Portal
General rights

Article

How Static Disorder Mimics Decoherence in Anisotropy Pump-Probe Experiments on Purple-Bacteria Light Harvesting Complexes

Clement Stross, Marc W Van der Kamp, Thomas A. A. Oliver,
Jeremy N Harvey, Noah Linden, and Frederick R. Manby

Just Accepted

1
2
3
4
5
6
7
8
9
10
11
12
13
14
15
16
17
18
19
20
21
22
23
24
25
26
27
28
29
30
31
32
33
34
35
36
37
38
39
40
41
42
43
44
45
46
47
48
49
50
51
52
53
54
55
56
57
58
59
60

How Static Disorder Mimics Decoherence in Anisotropy Pump-Probe Experiments on Purple-Bacteria Light Harvesting Complexes

Clement Stross,[†,‡] Marc W. Van der Kamp,[†] Thomas A. A. Oliver,[¶] Jeremy Harvey,[†,§] Noah Linden,[‡] and Frederick R. Manby[*,†]

Centre for Computational Chemistry, School of Chemistry, University of Bristol, Bristol BS8 1TS, UK, School of Mathematics, University of Bristol, Bristol BS8 1TW, UK, School of Chemistry, University of Bristol, Bristol BS8 1TS, UK, and Department of Chemistry, KU Leuven, Celestijnenlaan 200F, B-3001 Leuven

E-mail: fred.manby@bristol.ac.uk

---
[*]To whom correspondence should be addressed
[†]Centre for Computational Chemistry, School of Chemistry, University of Bristol, Bristol BS8 1TS, UK
[‡]School of Mathematics, University of Bristol, Bristol BS8 1TW, UK
[¶]School of Chemistry, University of Bristol, Bristol BS8 1TS, UK
[§]Department of Chemistry, KU Leuven, Celestijnenlaan 200F, B-3001 Leuven

1

Abstract

Anisotropy pump-probe experiments have provided insights into the character of excitons formed in photosynthetic complexes. Rapid decay in the observed anisotropy is cited as evidence of the strength of coupling of the excitonic degrees of freedom to their environment. Here we show that ensemble averaging over realistic model Hamiltonians leads to a rapid decay of anisotropy to a value close to the observed asymptote, and at a rate comparable to observed decay rates, even in the absence of coupling to the environment. While coupling to the environment will clearly play a role in the dynamics of such systems, our calculations suggest that caution is needed in deducing the strength of this coupling from anisotropy experiments. We also set out to clarify the nature quantum states and processes involved in the dynamics of such systems, and the associated terminology.

1 Introduction

Photosynthesis is the process by which energy in the form of sunlight is converted into the biomass of plants, and other organisms. Purple bacteria live in ponds, lakes, and streams in low-light conditions,[1] and have thus evolved intricate mechanisms and architectures for efficient energy capture and transport. The energy, initially absorbed by light harvesting complexes, is transported to a single reaction centre with near unit efficiency,[1–4] implying that the system is somehow constructed to minimize dissipative energy loss.

Two-dimensional electronic spectroscopy experiments[5–13] have been interpreted as showing long-lived coherences between excitonic states in photosynthetic light-harvesting complexes. This coherence has often been cited as an explanation of the remarkable exciton transfer directionality and efficiency, based on ideas such as quantum search algorithms[7,14] and noise-assisted transport.[15–20] However, the origin of oscillations in two-dimensional electronic spectra is still under debate, and while originally thought to be purely electronic[5–11,13] it is now increasingly attributed to vibrational wavepackets[21,22] or vibronic coherences.[12,23–25]

Many attempts have been made to model light harvesting complexes. It is known that the pigment-pigment and pigment-bath couplings are of similar orders,[26] meaning neither can be treated perturbatively. Hence the system is neither close to the Redfield[27] (strong electronic, weak bath coupling) nor Förster[28–30] (weak electronic, strong bath coupling) limits. This has led to the development of new methods such as the hierarchical equation of motion[31] and modified Redfield theory.[32] Another common approach is to assume that the dynamics in the excitonic subsystem is Markovian, and to model it using master equations in the Lindblad form.[18,19,33]

The peripheral antenna complexs of some light-harvesting purple bacteria are known as LHIIs. These are membrane-bound proteins containing two distinct rings of bacterio-chlorophyll-a (BChl) chromophores. Each ring has approximate C_N symmetry, and contain N and $2N$ chromophores. Complexes where $N = 8, 9, 10$ have been observed in nature,[34] and it has been suggested that these values of N maximise exciton transfer efficiency.[35] Our study focuses on LHII from the purple bacterium *Rhodopseudomonas acidophila* (strain 10050), because it is structurally[36] and spectroscopically well characterised.[34] For this system $N = 9$, and the rings with 9 and 18 chromophores are referred to as the B800 and B850 rings, denoting the wavelength of their respective absorption maxima.

Many groups have investigated exciton dynamics in LHII using femtosecond pump-probe spectroscopy.[37–43] The key observable is the anisotropy between signals with the probe pulse parallel and perpendicular to the pump pulse, as a function of the delay between the two pulses (see Sec. 4 below). This anisotropy rapidly decays from an initial value to a plateau at or a little below 1/10, on a timescale of around 50 fs. Such observations have been cited as evidence for dephasing and localisation of the exciton wave packet.[34,38–47]

One model often invoked to interpret anisotropy experiments is the circularly degenerate oscillator, in which the total anisotropy has an initial value of 3/10. The processes of pure dephasing and population exchange (see section 3) cause the anisotropy to decay to 2/10 and 1/10, respectively.[46,48,49] This has led to the interpretation that these processes are

responsible for the observed short-time anisotropy decay in LHII.

In this work we find that reasonable model Hamiltonians for the LHII B850 ring are very far from that of the circularly degenerate oscillator, and that the difference cannot be accounted for as a small perturbation. We use Hamiltonians with a realistic amount of disorder, but no explicit quantum mechanical coupling to the environment. Nevertheless the ensemble averaging over the static disorder leads to a rapid decay in anisotropy to a similar minimum value and at a similar rate to the experimental observations.

Obviously the exciton does couple to the environment, but our observations cast doubt on the legitimacy of *deducing* the strength of this coupling from anisotropy experiments, and in particular suggest that the observed anisotropy decay rate provides a lower bound, rather than a particular value, for the timescale associated with coupling to the environment.

2   Modelling LHII

We extract uncorrelated snapshots from molecular dynamics (MD) calculations to provide BChl geometries for quantum mechanical calculations; details are provided in the Supplementary Information.

2.1   Excitonic model Hamiltonian

A simple excitonic Hamiltonian with static disorder is used in an attempt to find a minimal description of experimental properties. Each chromophore is modelled as a two-level site with ground and excited states $|\phi_j^{(0)}\rangle$ and $|\phi_j^{(1)}\rangle$ separated by energy E_j. The ground state of the m-site complex is the product state $|\Phi^{(0)}\rangle = |\phi_1^{(0)} \cdots \phi_j^{(0)} \cdots \phi_m^{(0)}\rangle$ and the state $|\Phi_j\rangle$ with a single exciton at site j is $|\Phi_j\rangle = |\phi_1^{(0)} \cdots \phi_j^{(1)} \cdots \phi_m^{(0)}\rangle$.[50] States containing more than one exciton are not considered. The model Hamiltonian in the one-exciton manifold has the form

$$H = \sum_{j=1}^{m} E_j |\Phi_j\rangle\langle\Phi_j| + \sum_{j' \neq j} V_{jj'} |\Phi_j\rangle\langle\Phi_{j'}| \tag{1}$$

where $V_{jj'}$ is the coupling matrix element between excited states of sites j and j'.[50]

Assuming non-overlapping monomers, so that exchange effects can be neglected, the coupling matrix elements are given by

$$V_{jj'} = \iint \frac{\rho_j(\boldsymbol{r})\rho_{j'}(\boldsymbol{r'})}{|\boldsymbol{r} - \boldsymbol{r'}|} \, \mathrm{d}\boldsymbol{r} \, \mathrm{d}\boldsymbol{r'} \tag{2}$$

where ρ_j is the electronic transition density of monomer j.[51] For monomers that are well separated, the coupling matrix element is well approximated by the leading dipole-dipole term

$$V_{jj'} = \frac{\boldsymbol{\mu}_j \cdot \boldsymbol{\mu}_{j'}}{|\boldsymbol{r}_{jj'}|^3} - 3\frac{(\boldsymbol{\mu}_j \cdot \boldsymbol{r}_{jj'})(\boldsymbol{\mu}_{j'} \cdot \boldsymbol{r}_{jj'})}{|\boldsymbol{r}_{jj'}|^5} \tag{3}$$

where $\boldsymbol{\mu}_j$ is the transition dipole for monomer j and $\mathbf{r}_{jj'}$ is the vector between the Mg atoms of the two chromophores. Trial TDDFT and CIS calculations on selected BChl dimer structures suggest that while this equation does not describe the coupling with exact numerical detail, the qualitative behaviour is captured.[52,53] Improvements in the couplings can be made using such methods as frozen density embedding,[54,55] or by using higher-order multipole moments.[53] Kenny *et al.* investigated the accuracy of different methods for calculating the couplings, but found that given the size of the errors arising from uncertainties in crystallographic atomic coordinates, more computationally expensive methods for calculating the couplings are 'rarely justified'.[56]

The parameters E_j and $\boldsymbol{\mu}_j$ were computed using linear-response time-dependent density functional theory (TDDFT) as implemented in the Turbomole package.[57] Several exchange-correlation functionals and basis sets were tested for balance of accuracy and computational expense. It was found that the best cost to accuracy ratio was achieved with the hybrid functionals B3LYP[58] and PBE0[59] in the SVP basis set.[60] Using generalized-gradient approximation functionals, the character of the lowest excited state was not always correct.[61] The size of the basis set was found to have little effect, and increasing the basis set was found to be far less important than the use of hybrid density functionals.

The values of E_j and $\boldsymbol{\mu}_j$ were computed using PBE0/SVP for three sets of 250 uncorrelated BChl structures drawn from the molecular dynamics calculations, representing BChls from the two distinct α and β positions within the B850 ring, and from the B800 ring. The energies and transition dipole moment magnitudes are shown in Table 1. To account for interactions with the protein environment (and compensate for other sources of error) the energy distributions are shifted to match the experimental absorption maxima.

Table 1: Calculated distributions of excitation energies and transition-dipole magnitudes in atomic units for the BChls in the B850 and B800 rings of LHII. The calculations are performed using TDDFT at the PBE0/SVP level on 250 BChls. Subsequent calculations used the shifted energy mean shown, as described in the text.

	$\langle E \rangle$	$\langle E \rangle_{\text{shifted}}$	$\sigma(E)$	$\langle |\boldsymbol{\mu}| \rangle$	$\sigma(|\boldsymbol{\mu}|)$
B850-α	0.0688	0.0563	0.0012	2.863	0.064
B850-β	0.0692	0.0563	0.0013	2.828	0.068
B800	0.0691	0.0573	0.0012	2.874	0.072

Subsequent calculations were averaged over 3000 of uncorrelated MD snapshots. To avoid the expense of many thousands of TDDFT calculations, all subsequent values for E_j and μ_j, for a given geometry, are drawn at random from the distributions described above. The transition dipole vector $\boldsymbol{\mu}_j$ was aligned with the vector connecting opposite nitrogen atoms N_a and N_b of the chlorin ring (see Fig. 1).

2.2 Absorption spectrum

The one-exciton eigenstates of the Hamiltonian H are superpositions of the basis states

$$|\Psi_k\rangle = \sum_{j=1}^{m} c_{kj} |\Phi_j\rangle \tag{4}$$

and the intensity of the absorption from the ground state $|\Phi^{(0)}\rangle$ to the excited state $|\Psi_k\rangle$ is proportional to

$$I_k \propto E_k |\langle \Psi_k | \hat{\boldsymbol{\varepsilon}} \cdot \boldsymbol{\mu} | \Phi^{(0)} \rangle|^2 \tag{5}$$
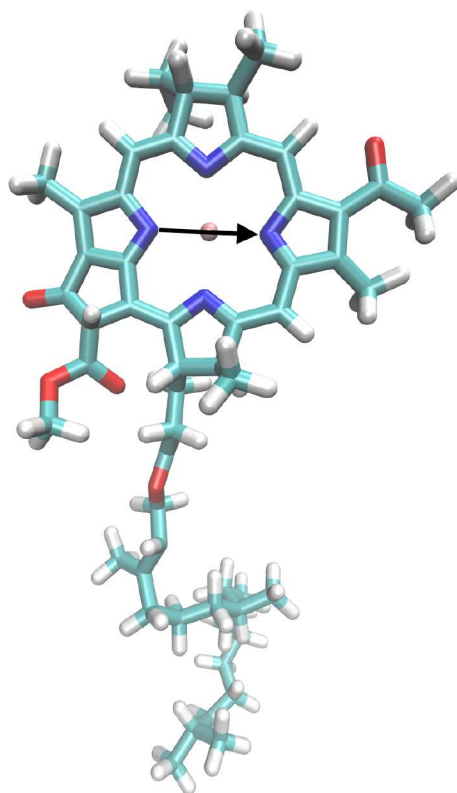
Figure 1: Bacteriochlorophyll chromophore with the direction of the transition dipole moment marked. Here this is modelled as the vector between the two nitrogen atoms indicated; the sign of the transition dipole moment vector is arbitrary.

where $E_k = \langle \Psi_k | H | \Psi_k \rangle$. Here $\hat{\boldsymbol{\varepsilon}}$ is the unit vector in the direction of the polarization of the incident light, and is chosen to have random orientation (which is equivalent to having a fixed light source and randomising the orientation of the LHII complex). Since all one-exciton states lie at approximately the same energy, we also neglect the energy factor E_k.

Expanding $\langle \Psi_k | \hat{\boldsymbol{\varepsilon}} \cdot \boldsymbol{\mu} | \Phi^{(0)} \rangle$ in the monomer basis we obtain

$$I_k \propto \left| \sum_{j=1}^{m} c_{kj} \, \hat{\boldsymbol{\varepsilon}} \cdot \boldsymbol{\mu}_j \right|^2 \tag{6}$$

where $\boldsymbol{\mu}_j$ is the transition dipole moment for a single BChl

$$\boldsymbol{\mu}_j = \langle \phi_j^{(1)} | \boldsymbol{\mu} | \phi_j^{(0)} \rangle \ . \tag{7}$$

The absorption spectrum is modelled by summing the calculated spectrum for 5000 geometries drawn from MD, and the resulting absorption spectrum is shown in Figure 2. The poor fit of the B800 ring is most likely due to the lack of the protein environment (specifically a coordinating histidine residue) in our TDDFT calculations. We would expect calculations that incorporated the effect of the protein environment to help improve this issue.[62]
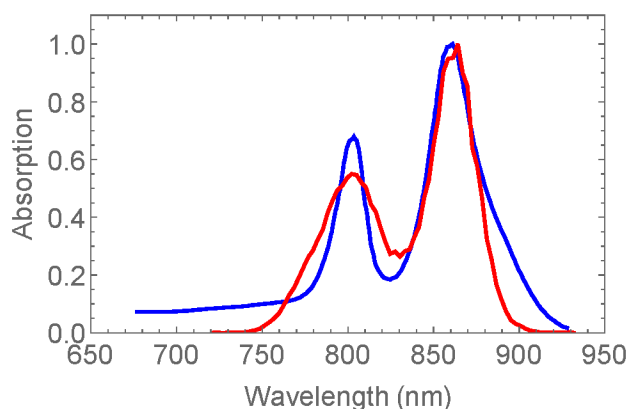
Figure 2: Computed absorption spectrum for the LHII complex in red, and the experimental spectrum in blue.[63] The energies of the BChls in the computed spectrum are from random distributions with means and standard deviations given by Table 1. Two parameters are used to shift the B850 and B800 excitation energies, compensating for protein effects and intrinsic DFT-based errors.

3 Terminology

Here we aim to clarify and distinguish between the wide variety of physical process and types of quantum states that are important in the study of photosynthetic systems. A particular challenge is that many of the terms, such as dephasing and decoherence, are used differently in different fields. In quantum information theory, decoherence and dephasing are sometimes used interchangeably,[64] whereas in spectroscopy they are sometimes given distinct meanings.[65–67]

3.1   A single system

It will be helpful to start with the notion of a pure state of a single system, described by a wavefunction $|\Psi\rangle$. The associated density matrix is

$$\rho = |\Psi\rangle \langle\Psi| \tag{8}$$

and has the property $\text{tr}\,\rho^2 = 1$. In dynamical processes that do not involve coupling between the system described by ρ and an environment, the density matrix ρ evolves unitarily, and hence the value of $\text{tr}\,\rho^2$ is preserved.

On the other hand, if the dynamics involves coupling to an environment, the value of $\text{tr}\,\rho^2$ can reduce. A state with $\text{tr}\,\rho^2 < 1$ is called *mixed*, and cannot be written in form of Eq. (8). We will call any process that changes the value of $\text{tr}\,\rho^2$ for a single system *decoherence*; a process that is the mechanism behind homogeneous broadening.

If there is a preferred basis, two principal types of decoherence can be distinguished. *Pure dephasing* is any process in which the off-diagonal elements in ρ (in this preferred basis) decay. (The term dephasing is used because the decay in the off-diagonal elements can arise by randomization of phases in a particular basis in a pure state.) *Population exchange* is change of the diagonal elements of the density matrix in the eigenbasis. It is often the case that population exchange has the effect that the diagonal elements tend towards a common value.

3.2   Ensembles of systems

For an ensemble of N non-interacting systems, the total density matrix is given by a tensor product of the individual density matrices

$$\rho_{\text{ens}} = \rho_1 \otimes \rho_2 \otimes \cdots \otimes \rho_N . \tag{9}$$

An ensemble observable O_{ens} is defined as

$$O_{\mathrm{ens}} = \sum_j O_j^{\mathrm{ens}}$$

$$O_j^{\mathrm{ens}} = \mathbb{I} \otimes \cdots \otimes O_j \otimes \cdots \otimes \mathbb{I}$$

(10)

where $\mathbb{I}$ is the identity operator. The expectation value for the observable is

$$\langle O_{\mathrm{ens}} \rangle = \mathrm{tr}\, \rho_{\mathrm{ens}} O_{\mathrm{ens}} = \sum_j \mathrm{tr}\, \rho_j O_j \ .$$

(11)

If the operators O_j are identical, we can further simplify the expectation value as

$$\langle O_{\mathrm{ens}} \rangle = \sum_j \mathrm{tr}\, \rho_j O = \mathrm{tr} \left(\sum_j \rho_j \right) O$$

(12)

(and a closely related expression applies if the operators O_j only differ from one another by unitary transformations). This expression can be interpreted in terms of an averaged density matrix

$$\rho_{\mathrm{av}} = \frac{1}{N} \sum_j \rho_j$$

and an ensemble expectation value give by $\langle O_{\mathrm{ens}} \rangle = N \, \mathrm{tr}\, \rho_{\mathrm{av}} O$. Despite having the correct properties (positivity and unit trace) it is important to recognise that ρ_{av} is not the density matrix of any physical system.

In situations where it is meaningful to define ρ_{av}, it is perfectly possible that $\mathrm{tr}\, \rho_{\mathrm{av}}^2 < 1$, even when the separate systems of the ensemble are described by pure states. A process in which the off-diagonal elements of $\mathrm{tr}\, \rho_{\mathrm{av}}^2$ reduce is called *ensemble dephasing*.

However we stress that the concept of ensemble dephasing is not always meaningful, because although it is obviously always possible to form an averaged density matrix, an ensemble observable can only be computed from it when the observable operators O_j are identical to one another (or related by a unitary transformation). This not always true for physically and experimentally relevant observables. For example, even though the dipole

operator is a uniquely defined quantum mechanical operator, its projections into the site bases of different instances of LHII structures are not generally equal (or equivalent within a unitary transform).

Localisation is often (but not here) used to describe dephasing (pure or ensemble) in the site basis, such that a state that is a mixture of site states is maximally localised. We avoid using this term in this way because it seems counterintuitive to describe a state in which there is equal probability of excitation at each site as 'localised'.

4   Anisotropy

In pump-probe experiments on LHII,[37–42] anisotropy effects are quantified by measuring the difference in absorption when the probe pulse has an electric vector parallel ($\tilde{\varepsilon}_{\parallel}$) or perpendicular ($\tilde{\varepsilon}_{\perp}$) to the electric vector ε of the pump laser. The key observables are the time-dependent absorption differences $\Delta A(t) = A(t) - A^{(0)}$, where $A(t)$ is the probe absorption measured a time t after the pump pulse, and $A^{(0)}$ is the absorption in the absence of the pump pulse. The anisotropy is then defined by:

$$r(t) = \frac{\Delta A_{\parallel}(t) - \Delta A_{\perp}(t)}{\Delta A_{\parallel}(t) + 2\Delta A_{\perp}(t)} \ . \tag{13}$$

The experimentally measured anisotropies $r(t)$ arise from averaging over an ensemble of distinct LHII complexes at random orientations. In our calculations, each LHII is characterized by a Hamiltonian (H) and an orientation (θ), and is associated with anisotropy $r_{H,\theta}(t)$. Averaging over orientations produces

$$r_H(t) = \langle r_{H,\theta}(t) \rangle_{\theta}$$

and further averaging over different Hamiltonians gives

$$r(t) = \langle r_H(t) \rangle_H \ .$$

Note that although the notation implies averaging of the anisotropies themselves, in both cases the averaging is actually performed on the absorption coefficients from which the anisotropies are calculated.

Later (Section 4.3) we will discuss how to calculate $\Delta A(t)$ for a single LHII complex. In Sections 4.1 and 4.2 we will discuss how the anisotropy is often interpreted using the model of a perturbed circularly degenerate oscillator.

4.1   Modelling LHII as a circularly degenerate oscillator

LHII (and similar systems) are commonly modelled using a Hamiltonian with circular symmetry, possibly with a small perturbation.[38,68–71] A system with m-fold rotational symmetry (for even m) has $m/2 - 1$ degenerate pairs of eigenstates, with non-degenerate states of lowest and highest energy. If the monomer transition dipoles are in the plane, only two of the m eigenstates are coupled to the (zero-exciton) ground state through transition dipoles. The two states in question are the lowest degenerate pair $|k = \pm 1\rangle$, and have transition dipoles perpendicular to one another. Here we label these states $|x\rangle$ and $|y\rangle$, and will refer to the system as a circularly degenerate oscillator. Perturbation through interaction with an environment can cause decoherence, and/or remove the energy degeneracy between the $|x\rangle$ and $|y\rangle$ states by an amount ΔE_{xy}.

In most studies of decoherence,[46,48,49] the Hamiltonian has degenerate $|x\rangle$ and $|y\rangle$ states (i.e. $\Delta E_{xy} = 0$). In this case ensemble averaging is trivial as all Hamiltonians are identical, so $r(t) \equiv r_H(t)$. Under this assumption, but including orientational averaging, the anisotropy

arising from the stimulated emission process is[48]

$$r^{\text{SE}}(t) = \frac{1 + 3e^{-2\Gamma t} + 3e^{-(2\Gamma+\gamma)t}}{10} \, . \tag{14}$$

The anisotropy from the ground-state bleaching is $r^{\text{GSB}} = 1/10$, and the total observable anisotropy can be shown to be (see Appendix A)

$$r(t) = \frac{1 + e^{-2\Gamma t} + e^{-(2\Gamma+\gamma)t}}{10} \, . \tag{15}$$

Here 2Γ is the rate of population exchange, defined as the rate at which the density matrix tends to $\rho_{\text{exch}} = (|x\rangle\langle x| + |y\rangle\langle y|)/2$ and γ refers to the rate of pure dephasing.[48,72]

This analysis — for the case of degenerate states $|x\rangle$ and $|y\rangle$ — shows that the dephasing process can reduce the stimulated emission anisotropy to $2/5$ ($\gamma \neq 0$ and $\Gamma = 0$). Dephasing alone cannot give rise to an anisotropy of $1/10$ (around the typical value observed in many experiments); it is only with the population exchange rate $\Gamma \neq 0$ that a total anisotropy of $1/10$ can be obtained. This model does predict the double-exponential decay observed in experiments, but fails to account for the measured anisotropy falling below $1/10$.

4.2   Modelling LHII as a perturbed circular oscillator

Coupling to the environment or some other perturbation may open an energy gap ΔE_{xy} between the $|x\rangle$ and $|y\rangle$ states. As before, the anisotropy for an orientationally averaged perturbed circular oscillator arises from the combination of ground-state bleaching and stimulated emission. Ground-state bleaching alone would produce the time and energy-gap independent anisotropy $r_H^{\text{GSB}} = 1/10$, and stimulated emission alone would lead to the anisotropy[73]

$$r_H^{\text{SE}}(t, \Delta E_{xy}) = \frac{4 + 3\cos(\Delta E_{xy}t/\hbar)}{10}. \tag{16}$$

The anisotropy incorporating both effects is (see Eq. (8) of Ref. 68)

$$r_H(t, \Delta E_{xy}) = \frac{2 + \cos(\Delta E_{xy} t/\hbar)}{10} \ .$$ (17)

These results can be obtained by following the procedure described in Appendix A.

Ensemble averaging in this model amounts to averaging over values of ΔE_{xy}. The anisotropies arising from the averaged absorption coefficients can then be expressed as a weighted average over the anisotropies $r_H(t, \Delta E_{xy})$.[74] For $t = 0$ the cosine terms in Eq. 17 are all unity, so the initial anisotropy is $r(t = 0) = 3/10$. For large t, the weighted average over cosines with different frequencies vanishes, leading to an asymptotic anisotropy of $r(t \to \infty) = 1/5$. The time scale of the decay in this model is purely determined by the distribution of values of ΔE_{xy}, and has no connection to decoherence.

It is important to note that the same long-time anisotropy of $1/5$ can be obtained either by ensemble averaged, pure-state calculations on perturbed circular oscillators; or by dephasing of a single circularly degenerate oscillator. Both models produce exponential decay in the anisotropy from $3/10$ to $1/5$, in contrast to the experimental double exponential decay and the long-time value of around 0.1. This has been interpreted as evidence for dephasing and population exchange.[34,38–47]

In this work we use a model of the type above, with no decoherence, but with a realistic ensemble of LHII Hamiltonians. We find that we do not need to invoke decoherence to reproduce the majority of the observed experimental behaviour, and that the perturbed circular oscillator is not a suitable model for LHII. As we will see, the degree of disorder cannot be considered as a small perturbation; the eigenvalues cannot be approximately arranged into near-degenerate pairs; and many more than two states have significant transition-dipole coupling to the zero-exciton ground state.

4.3 Model of Anisotropy

The system is initially in the ground state $|\Phi^{(0)}\rangle$. After interaction with the pump pulse, time-dependent perturbation theory determines the state to be:

$$|\Psi(t=0)\rangle = c_0|\Phi^{(0)}\rangle + R|\Phi^{(0)}\rangle \tag{18}$$

where R is the operator representing interaction with the light source, and

$$|c_0|^2 = 1 - \||R|\Phi^{(0)}\rangle\|^2 \tag{19}$$

The interaction with the radiation in the semiclassical approximation is

$$R = \lambda \sum_k |\Psi_k\rangle \rho^{1/2}(E_k)\langle\Psi_k| \, \boldsymbol{\varepsilon} \cdot \boldsymbol{\mu} \tag{20}$$

where λ is a positive real parameter which accounts for experimental conditions such as field strength, and is sufficiently small that R can be treated perturbatively. The energy density of the laser pulse is given by ρ, the (normalized) field vector by $\boldsymbol{\varepsilon}$ and the dipole operator by $\boldsymbol{\mu}$.

We later refer to the state $|\Psi(t)\rangle$, which is obtained through the time-dependent Schrödinger equation:

$$|\Psi(t)\rangle = e^{-iHt}|\Psi(t=0)\rangle \, . \tag{21}$$

It will be convenient to define a normalized state representing the excited portion of $|\Psi(t=0)\rangle$:

$$|\Psi_e(t=0)\rangle = \frac{R|\Phi^{(0)}\rangle}{\||R|\Phi^{(0)}\rangle\|} \tag{22}$$

and we will define wavefunction parameters δ_k such that

$$R|\Phi^{(0)}\rangle = \sum_k \delta_k|\Psi_k\rangle \, . \tag{23}$$

The experiments consist in measuring absorption through a probe pulse described by an operator

$$\tilde{R} = \tilde{\lambda} \sum_k |\Psi_k\rangle \tilde{\rho}^{1/2}(E_k) \langle \Psi_k| \, \tilde{\boldsymbol{\varepsilon}} \cdot \boldsymbol{\mu} \, . \tag{24}$$

We also define the corresponding normalized excited-state wavefunction

$$|\tilde{\Psi}_e\rangle = \frac{\tilde{R}|\Phi^{(0)}\rangle}{\|\tilde{R}|\Phi^{(0)}\rangle\|} \tag{25}$$

and associated wavefunction parameters $\tilde{\delta}_k$

$$\tilde{R}|\Phi^{(0)}\rangle = \sum_k \tilde{\delta}_k |\Psi_k\rangle \, . \tag{26}$$

Differences in absorption are observed with and without the pump pulse, and the observed absorption consists of three contributions:

$$\Delta A(t) = A^{\text{GSA}} - A^{(0)} + A^{\text{SE}}(t) \tag{27}$$

where

$$A^{(0)} = |\langle \tilde{\Psi}_e| \tilde{R}|\Phi^{(0)}\rangle|^2 \tag{28a}$$

$$A^{\text{GSA}} = |\langle \tilde{\Psi}_e| \tilde{R}|\Psi(t)\rangle|^2 \tag{28b}$$

$$A^{\text{SE}}(t) = -|\langle \Phi^{(0)}| \tilde{R}^\dagger|\Psi(t)\rangle|^2 \, . \tag{28c}$$

The term $A^{(0)}$ is the absorption from the ground state $|\Phi^{(0)}\rangle$ in the absence of the pump pulse. After interacting with the pump pulse, a fraction $|c_0|^2$ of the complexes remain in the ground state, and contribute an absorption A^{GSA}. The value $A^{\text{GSB}} = A^{\text{GSA}} - A^{(0)}$ is known as ground-state bleaching, and is negative as $A^{\text{GSA}} < A^{(0)}$ due to the pump reducing the ground state population. In principle A^{GSB} could depend on time, but in fact does not

do so as $|c_0|^2$ is time independent. Finally, if the complex is excited, the pump pulse can induce stimulated emission, resulting in the additional negative absorption contribution A^{SE}. Excited state absorption is not included in this study, although a framework to model it can be derived.[40,47,68,74,75]

Each contribution can be computed directly using the previous equations:

$$A^{(0)} = \sum_k |\tilde{\delta}_k|^2 \tag{29a}$$

$$A^{\mathrm{GSA}} = \left[1 - \sum_k |\delta_k|^2\right] \sum_k |\tilde{\delta}_k|^2 \tag{29b}$$

$$A^{\mathrm{SE}}(t) = -\left|\sum_k \tilde{\delta}_k^* \delta_k \, e^{-iE_k t/\hbar}\right|^2 \tag{29c}$$

and the total observed absorption is given by

$$\Delta A(t) = -\sum_k |\delta_k|^2 \sum_k |\tilde{\delta}_k|^2 - \left|\sum_k \tilde{\delta}_k^* \delta_k \, e^{-iE_k t/\hbar}\right|^2 . \tag{30}$$

This is computed for the two cases of parallel $\Delta A_\parallel(t)$ ($\tilde{\varepsilon} \cdot \varepsilon = 1$) and perpendicular $\Delta A_\perp(t)$ ($\tilde{\varepsilon} \cdot \varepsilon = 0$) laser pulses.

Each δ_k is proportional to λ, and $\tilde{\delta}_k$ to $\tilde{\lambda}$. The absorption $\Delta A(t)$ is proportional to $\lambda^2 \tilde{\lambda}^2$, so depends on experiment-specific based parameters. The anisotropy, a ratio of absorptions, has no dependence on λ or $\tilde{\lambda}$ so can be numerically compared between different experiments and simulations.

Anisotropies are computed according to

$$r(t) = \frac{\sum_{H,\theta} \Delta A_\parallel(t) - \sum_{H,\theta} \Delta A_\perp(t)}{\sum_{H,\theta} \Delta A_\parallel(t) + 2\sum_{H,\theta} \Delta A_\perp(t)} \tag{31}$$

where the sum $\sum_{H,\theta}$ represents a sum over the Hamiltonians of different LHII complexes each in random orientations with respect to the pump-probe set up. The energy densities of the pump and probe laser pulses ($\rho(E)$ and $\tilde{\rho}(E)$) are modelled as Gaussians with mean and

width as described in the experimental work of Kennis *et al.*[37] The pump and probe pulses have energies centred at 860 nm and 870 nm (0.0530 and 0.0524 hartree) respectively, and both have standard deviations of 38 nm (2.62 millihartree). Results from other experimental setups are shown in Table 2.

5 Results and Discussion

Analysis of LHII as a circularly degenerate oscillator implies that the experimentally observed anisotropy decay can be interpreted in terms of pure dephasing and population-exchange timescales. This interpretation relies on the quality of the circularly degenerate oscillator model of exciton dynamics in LHII; and as we have seen, even a small perturbation that lifts the degeneracy between $|x\rangle$ and $|y\rangle$ leads to an ensemble averaging effect that can mask the decoherence timescales (see Section 4.2).

The model Hamiltonians calculated in this work are in fact very far from the circularly degenerate case, and well beyond the regime accessible by perturbation theory, casting doubt on the utility of using these models to interpret anisotropy experiments on the LHII system. The eigenspectra of the Hamiltonians bear no resemblance to the spectrum of the circularly degenerate oscillator (see Figure 3), and there are significant transition dipoles to many of the eigenstates (see Figure 4). For these reasons, many eigenstates are populated during the pump-probe experiment, as illustrated in Figure 5. In these calculations we have focused purely on differences in chromophore structures, and in their relative positions. Effects that we have neglected — such as fluctuations in the electric field due to motion in the protein environment, and the influence of the bacterial membrane on the dynamics of the protein — will certainly influence the detailed nature of the static noise in the excitonic Hamiltonian. But it is unlikely that these effects would change our overall conclusion given that the broadening of the experimental absorption spectrum is reasonably well reproduced by our calculations.
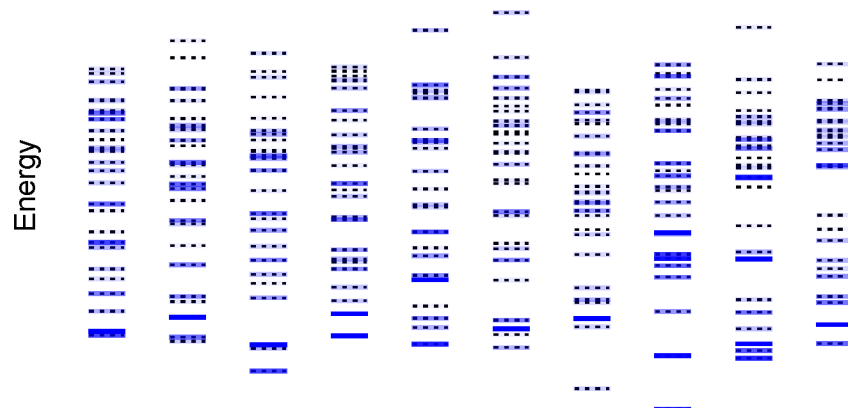
Figure 3: Eigenvalue spectra of a representative selection of computed LHII Hamiltonians used in this work. The black dotted line shows the energy of each state, and the thickness of the overlaid coloured lines are proportional to $|\boldsymbol{\mu}_k \cdot \boldsymbol{\varepsilon}|$, which are normalised to the highest value for each Hamiltonian and orientation. It can be seen the physically realistic spectra are very far from the circularly degenerate oscillator case where only two states absorb. There is also clearly no vestige of the degenerate eigenvalue ladder that would be expected for a circular oscillator. This arises because the disorder is of a similar magnitude to the inter-site couplings.

Three examples of the anisotropy profiles for individual LHII complexes are shown in Figure 6. The LHII complexes are orientated randomly with respect to the pump-probe pulses, have geometries drawn from MD, and BChl site energies chosen from a distribution as described above. Also shown is the inverse participation[34] measure for delocalisation, defined by

$$P(t)^{-1} = \frac{[\sum_j | \langle \Phi_j | \Psi_e(t) \rangle |^2]^2}{\sum_j | \langle \Phi_j | \Psi_e(t) \rangle |^4}, \tag{32}$$

which indicates the number of chromophore sites that participate in the state at time t. As noted before (Section 3), the term localisation is sometimes used to mean dephasing in the site basis, we do not use that definition here.

The ensemble behaviour of many LHII complexes, each with different relative orientations with respect to the polarisation of the pump-probe laser beams, is shown in Figure 7. Our simulated ensemble anisotropy calculations reproduce the experimental decay timescale, giving a decay constant of 17.4 fs, despite not including decoherence (as defined in our paper) in our model. However the anisotropy approaches a value around 0.13 rather than ≈ 0.1 as seen
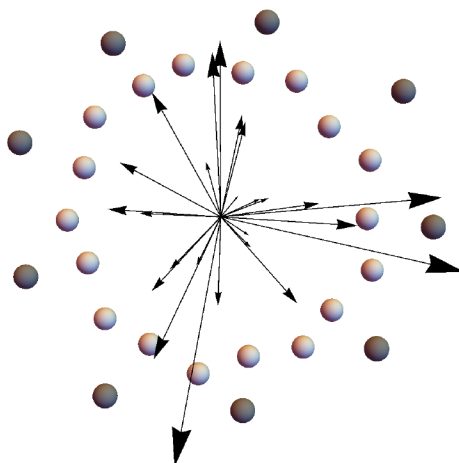
Figure 4: Transition dipole moments between the (zero-exciton) ground state and the 27 eigenstates of a Hamiltonian used in this work. The spheres mark Mg positions within each chlorophyll for the MD snapshot used to generate the Hamiltonian. All transition dipole vectors are drawn originating at the centre of mass of the LHII.
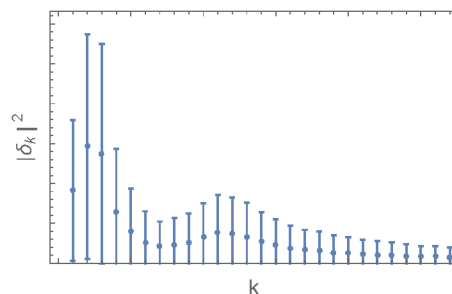
Figure 5: The mean value of the absorption coefficients for the 3000 LHII Hamiltonians used in this work, with error bars representing the standard deviation (not the standard error). The eigenstates k are ordered in increasing energy. It can be seen that with realistic Hamiltonians many more states are excited by the radiation than the two that participate in the circularly degenerate oscillator. Here the radiation density $\rho(E) = 1$.

in experiments (see Table 2). We fit to a single exponential rather than a bi-exponential, as used in experimental studies. Both discrepancies arise because we are only modelling ensemble (or inhomogeneous) effects; our model does not decsribe the population exchange process which leads to the longer experimental decay rate.

The timescale we observe in our calculated anisotropy decay is of course dependent on the magnitude of the static noise (or strength of inhomogeneous broadening). However this magnitude was computed directly, as described in Section 2, rather than fitted to produce the

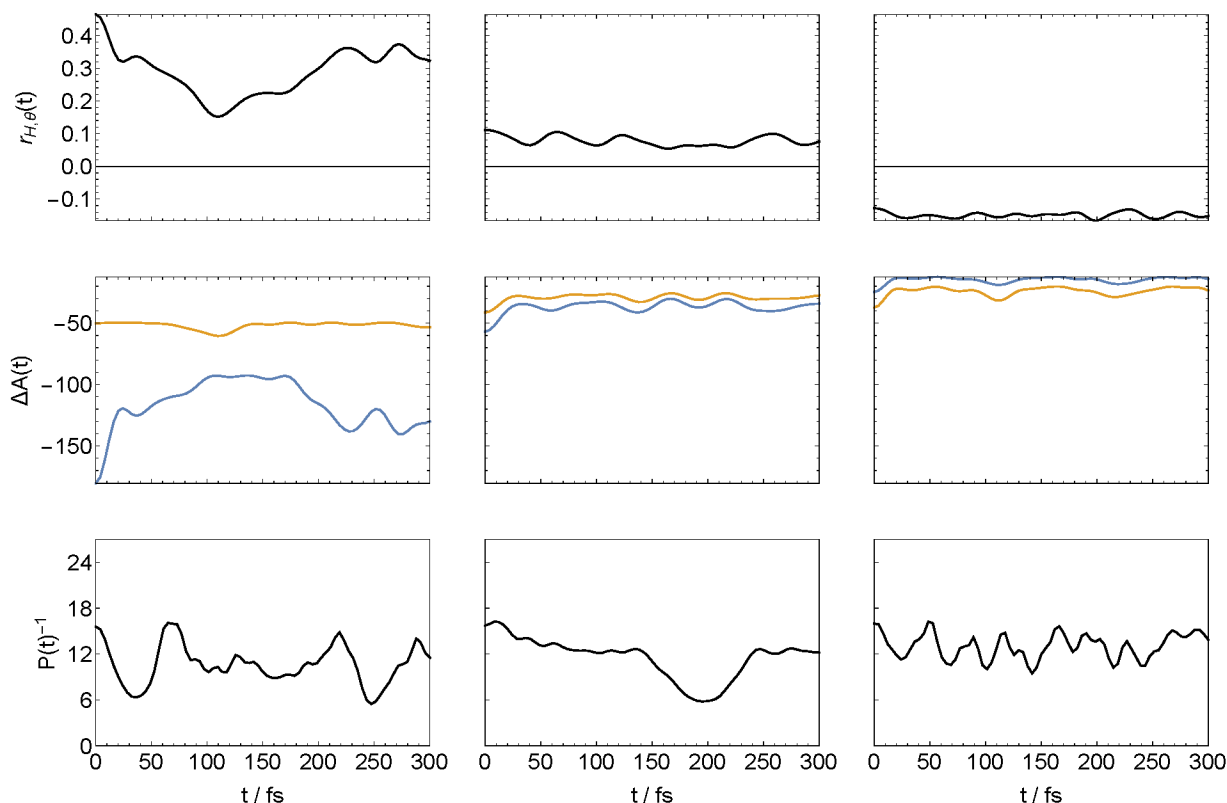Figure 6: Three examples of anisotropy (top); absorbance (middle; $\Delta A_\parallel$ in blue and $\Delta A_\perp$ in yellow) in arbitrary units; and exciton delocalisation (bottom; calculated using Eq. 32) for individual LHII complexes from randomly selected MD snapshots.

experimental decay rate. The experimentally observed anisotropy decay rate *may* provide information on the strength of homogeneous broadening, but a key message of our study is that this is not necessarily the case.

Pump-probe anisotropy experiments have been previously modelled using Förster theory[38,44,45,70] and Redfield theory.[47,75] These methods often conclude that dephasing and population exchange are relevant, and that the decoherence length (defined in various ways) of the exciton is around 4 BChl units.[44,45,70] We find that the average delocalisation length (defined through inverse participation) of the exciton is around 12 BChl units and does not substantially change with time. The localisation of the exciton in previous studies is caused by interaction with a bath, which is not present in our study.

Our results (Figure 7) show an anisotropy plateaus of around 0.13, lower than the 1/5
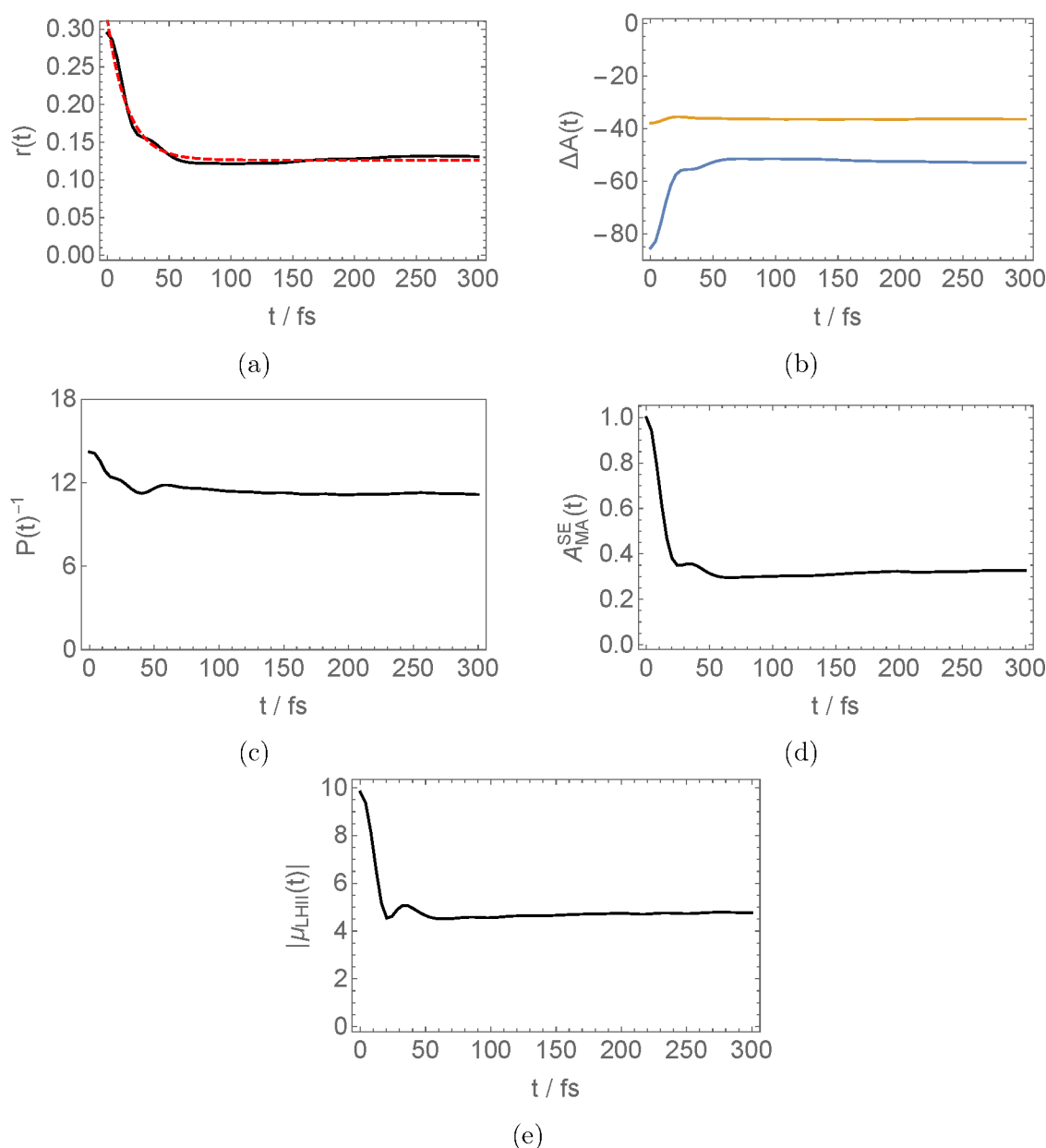
Figure 7: Anisotropy properties averaged over 3000 LHII conformations generated from MD, illustrating that the experimentally observed timescale can be reproduced by an ensemble of pure states. The anisotropy reaches a plateau slightly above the experimental value of 0.1, and is better fit to a single rather than a double exponential. (a) Average anisotropy of LHIIs (black) with a fit (red dashed) to $r_\infty + r_1 e^{-t/\tau_1}$ with $r_\infty = 0.126$, $r_1 = 0.187$, $\tau_1 = 16.4$ fs. (b) Average absorption $\Delta A_\parallel$ in blue and $\Delta A_\perp$ in yellow (arbitrary units). (c) Delocalisation of the exciton using the measure given in Eq. 32. (d) Excited-state stimulated emission at the magic angle, normalised such that $A_{\text{MA}}^{\text{SE}}(0) = 1$. (e) The average magnitude of the LHII transition dipole moment, this is plotted in units of $\langle |\boldsymbol{\mu}| \rangle$, the magnitude of the average transition dipole moment for the single BChls.

Table 2: Comparison of experimental pump-probe anisotropy results for various purple bacteria LHII complexes (top rows) with our work (bottom row). The parameters r_1, r_2, r_∞, t_1 and t_2 refer to the anisotropies and timescales for biexponential fits (see text). Values marked $*$ relate to fitting to a Gaussian decay, rather than an exponential.

λ / nm		r_1	t_1/fs	r_2	t_2/fs	r_∞	Ref.	
pump	probe							
860	870		< 100		< 100	0.1	37	*Rps. acidophila*
860	874	0.207	100	0.012	700	0.07	41	*Rps. acidophila*
860	940	0.21	90	0.04	410	0.1	38	*R. sphaeroides*
860	872	0.21	31	0.13	82.3	0.09	40	*R. sphaeroides*
851	845	0.124*	45*	0.176	116	0.110	42	*R. sphaeroides*
860	870	0.187	16.4			0.126		*Rps. acidophila*

predicted through an ensemble of perturbed circular oscillators (Section 4.2). This is because the environmental perturbation not only gives the energy difference ΔE_{xy} between the $|x\rangle$ and $|y\rangle$ states, but also results in many other eigenstates having non-zero transition dipole magnitudes and therefore becoming occupied (see Figure 5). This causes the ratio of A^{SE} to A^{GSB} to reduce (see Appendix B), in turn reducing the effect of stimulated emission and shifting the anisotropy towards the ground-state bleaching value.

This analysis does not explain how anisotropies below 0.1 are observed. The effects of excited-state absorption are not currently included in our analysis, but have been studied elsewhere.[40,47,68,74,75] Excited-state absorption, where absorbtion of a probe photon accesses the two-exciton manifold might further reduce the anisotropy to a value below 0.1.

It has been shown that for a system whose eigenstates are delocalized (for example, a circularly degenerate system), the transition dipole $\langle\Phi^{(0)}|\boldsymbol{\mu}|\Psi_e(t)\rangle$ is proportional to $N^{1/2}$, where N is the number of monomers over which the coherent excitation $|\Psi_e(t)\rangle$ has significant amplitude.[76,77] Stimulated emission at the magic angle $A_{\mathrm{MA}}^{\mathrm{SE}} = (A_{\parallel}^{\mathrm{SE}}+2A_{\perp}^{\mathrm{SE}})/3$ is proportional to $|\langle\Phi^{(0)}|\boldsymbol{\mu}|\Psi_e(t)\rangle|^2$. A decay in $A_{\mathrm{MA}}^{\mathrm{SE}}$ has thus been associated with a decay in N, or in other words with increasing localization.[42,44,78] As we have emphasised, the Hamiltonians used in this work do not resemble circularly degenerate oscillators, and as such the observed decay

in $A_{\mathrm{MA}}^{\mathrm{SE}}$ and $\langle \Phi^{(0)} | \boldsymbol{\mu} | \Psi_e(t) \rangle$ (Figure 7) are not associated with a substantial change in the inverse participation ratio or the onset of decoherence.

In the warm, wet, noisy environment of the experimental studies, decoherence will clearly play a role. However it does not seem possible to unequivocally deduce timescales for dephasing and population exchange from anisotropy decay, because ensemble averaging over realistic model Hamiltonians, in the absence of either decoherence effect, produces anisotropy decay with a similar timescale. This 'fake decoherence' effect[65,66] may mask the true timescale for decoherence.

6 Conclusion

The question of what happens to the energy immediately after an absorption event in LHII is of pressing importance to the understanding the initial charge separation rate and yield in photosynthesis. Pump-probe spectroscopic anisotropy show a characteristic double-exponential decay in observed anisotropies. The decay is often interpreted as arising from the decoherence of the exciton state as a result of coupling between an individual LHII complex and the bath. Analysis using the circularly degenerate oscillator model suggests a mapping from the two experimentally observed decay constants to the effects of pure dephasing and population exchange, so anisotropy pump-probe experiments have been used to provide estimates of these timescales.

Here we have set out to make model Hamiltonians by combining results of molecular dynamics and TDDFT calculations, and have found that the eigenvalue spectra of these Hamiltonians are very far removed from the spectrum of a symmetric circular system. The characteristic feature of degenerate pairs of eigenvalues is completely lost as a result of disorder, and the (zero-exciton) ground state is coupled to many (rather than just two) of the eigenstates.

We have found that ensemble averaging over these more realistic model Hamiltonians

leads to a rapid decay of anisotropy to a value close to the observed asymptote, and at a rate comparable to observed decay rates, *in the absence of any decoherence effects.* The difference between the anisotropy decay (exponential vs bi-exponential) and asymptotic values (0.13 vs 0.1) in our calculations and the prior experimental studies,[37–42] can be attributed to our deliberate lack of explicit coupling to an environmental bath. Such a coupling would result in pure dephasing and more importantly population exchange, which would add an additional slow decay component to our anisotropy, and lead to the long time value of 0.1.

Crucially we have shown that the faster observed decay component may not in fact relate to decoherence effects at all, but rather could arise from the ensemble averaging over a disordered sample of instantaneous LHII structures. Thus anisotropy experiments could be viewed as providing a lower bound to the decoherence timescale.

In 2D photon-echo experiments by Harel *et al.*[10] the decoherence time for the LHII was found to be between 55–90 fs. This time scale varied depending on the wavelength of the pump pulses. This is longer than the time constant for the anisotropy decay, originating from ensemble averaging, calculated in this work, and further suggests that the decoherence timescale is masked by ensemble averaging in anisotropy experiments.

Acknowledgements

A Calculations of Anisotropy for A Circular Oscillator

We wish to show how the anisotropy is calculated for a circular oscillator under different environmental perturbations. One such perturbation is decoherence which cannot be described in a wavefunction formalism. As such we must put each part of Equation 28 into density matrix form. For the background absorption $A^{(0)} = |\langle \tilde{\Psi}_e | \tilde{R} | \Phi^{(0)} \rangle|^2$ and using the definition in Equation 25 that $|\tilde{\Psi}_e\rangle = \tilde{R} |\Phi^{(0)}\rangle / \|\tilde{R} |\Phi^{(0)}\rangle\|$ we obtain

$$A^{(0)} = \left| \frac{\langle \Phi^{(0)} | \tilde{R}^\dagger \tilde{R} | \Phi^{(0)} \rangle}{\|\tilde{R} |\Phi^{(0)}\rangle\|} \right|^2$$
$$= \langle \Phi^{(0)} | \tilde{R}^\dagger \tilde{R} | \Phi^{(0)} \rangle \tag{33}$$
$$= \operatorname{tr} \tilde{R} |\Phi^{(0)}\rangle \langle \Phi^{(0)}| \tilde{R}^\dagger$$

The ground-state absorption is given by $A^{\mathrm{GSA}} = |\langle \tilde{\Psi}_e | \tilde{R} | \Psi(t) \rangle|^2$ where $|\Psi(t)\rangle = c_0 |\Phi^{(0)}\rangle + U(t) R |\Phi^{(0)}\rangle$ (Equation 18). Here $U(t)$ is the Hamiltonian unitary propagation operator, advancing the state to time t. The coefficient $c_0 = \sqrt{1 - \|R |\Phi^{(0)}\rangle\|^2}$, and is the probability amplitude of being in the ground state after the pump. We now note that (using the definition of R and $\tilde{R}$ in Equations 20 and 24) $\tilde{R} U(t) R |\Phi^{(0)}\rangle = 0$ as both R and $\tilde{R}$ excite the system. Therefore

$$A^{\mathrm{GSA}} = c_0^2 |\langle \tilde{\Psi}_e | \tilde{R} | \Phi^{(0)} \rangle|^2$$
$$= c_0^2 \left| \frac{\langle \Phi^{(0)} | \tilde{R}^\dagger \tilde{R} | \Phi^{(0)} \rangle}{\|\tilde{R} |\Phi^{(0)}\rangle\|} \right|^2$$
$$= c_0^2 \operatorname{tr} \tilde{R} |\Phi^{(0)}\rangle \langle \Phi^{(0)}| \tilde{R}^\dagger \tag{34}$$
$$= \left(1 - \operatorname{tr} R |\Phi^{(0)}\rangle \langle \Phi^{(0)}| R^\dagger \right) \operatorname{tr} \tilde{R} |\Phi^{(0)}\rangle \langle \Phi^{(0)}| \tilde{R}^\dagger .$$

So the ground-state bleaching value is

$$A^{\mathrm{GSB}} = A^{\mathrm{GSA}} - A^{(0)} = -\operatorname{tr} R |\Phi^{(0)}\rangle \langle \Phi^{(0)}| R^\dagger \operatorname{tr} \tilde{R} |\Phi^{(0)}\rangle \langle \Phi^{(0)}| \tilde{R}^\dagger , \tag{35}$$

which is time-independent as expected; it is also independent of any decoherence in the excited state. For the stimulated emission term we have

$$A^{\text{SE}}(t) = - \langle \Phi^{(0)} | \tilde{R}^\dagger | \Psi(t) \rangle \langle \Psi(t) | \tilde{R} | \Phi^{(0)} \rangle$$
$$= -\text{tr}\, \tilde{R}^\dagger\, U(t)\, R\, | \Phi^{(0)} \rangle \langle \Phi^{(0)} | R^\dagger\, U^\dagger(t)\, \tilde{R} | \Phi^{(0)} \rangle \langle \Phi^{(0)} | \tag{36}$$

again using the definition of $|\Psi(t)\rangle$ as before, but now using the property that $\tilde{R}^\dagger |\Phi^{(0)}\rangle = 0$.

We can use these new expressions to show the effect over time on absorption from dephasing and population exchange. The ground-state bleaching term is clearly independent of decoherence as it is time-independent. Stimulated emission $A^{\text{SE}}(t)$ contains a propagation term (i.e. $U(t)\rho U^\dagger(t)$ where $\rho = R\,|\Phi^{(0)}\rangle \langle \Phi^{(0)}|\, R^\dagger$) so time-dependent effects such as decoherence play a role.

For a circular oscillator Equation 20 gives

$$R = \lambda\mu\Big(\varepsilon_x\, |x\rangle \langle \Phi^{(0)} | + \varepsilon_y\, |y\rangle \langle \Phi^{(0)} | \Big)\,, \tag{37}$$

where $\mu\,\varepsilon_x = \langle x |\, \boldsymbol{\varepsilon} \cdot \boldsymbol{\mu}\, | \Phi^{(0)} \rangle$, with μ being the magnitude of the transition dipole moment (for both the x and y transitions), and ε_x being the component of the electric vector in the direction of the $|\Phi^{(0)}\rangle \rightarrow |x\rangle$ transition dipole moment. Likewise, Equation 24 gives

$$\tilde{R} = \tilde{\lambda}\mu\Big(\tilde{\varepsilon}_x\, |x\rangle \langle \Phi^{(0)} | + \tilde{\varepsilon}_y\, |y\rangle \langle \Phi^{(0)} | \Big)\,. \tag{38}$$

where now $\mu\,\tilde{\varepsilon}_x = \langle x |\, \tilde{\boldsymbol{\varepsilon}} \cdot \boldsymbol{\mu}\, | \Phi^{(0)} \rangle$, and $\tilde{\boldsymbol{\varepsilon}}$ is the probe polarisation and can be parallel ($\boldsymbol{\varepsilon} \cdot \tilde{\boldsymbol{\varepsilon}}_\parallel = 1$) or perpendicular ($\boldsymbol{\varepsilon} \cdot \tilde{\boldsymbol{\varepsilon}}_\perp = 0$) to the pump polarisation.

We can find the ground-state bleaching contribution to the absorption directly, as this is independent of any excited-state dynamics, using Equation 35:

$$A^{\text{GSB}} = -\lambda^2 \tilde{\lambda}^2 |\mu|^4 (\varepsilon_x^2 + \varepsilon_y^2)(\tilde{\varepsilon}_x^2 + \tilde{\varepsilon}_y^2)\,. \tag{39}$$

The electric vectors can be expressed as

$$
\boldsymbol{\varepsilon} = \tilde{\boldsymbol{\varepsilon}}_\parallel = \begin{pmatrix} \sin(\theta)\cos(\phi) \\ \sin(\theta)\sin(\phi) \\ \cos(\theta) \end{pmatrix} \qquad \tilde{\boldsymbol{\varepsilon}}_\perp = \begin{pmatrix} \cos(\theta)\cos(\chi)\cos(\phi) - \sin(\chi)\sin(\phi) \\ \cos(\theta)\cos(\chi)\sin(\phi) + \sin(\chi)\cos(\phi) \\ -\sin(\theta)\cos(\chi) \end{pmatrix} , \qquad (40)
$$

where θ and ϕ are evenly sampled from the unit sphere, and χ is an additional angle to sample over all vectors perpendicular to $\boldsymbol{\varepsilon}$. Then we average the different absorption properties over all solid angles using

$$
\langle A_\parallel \rangle = \frac{\int_0^\pi d\theta \int_0^{2\pi} d\phi \; A_\parallel(\theta, \phi)\sin\theta}{\int_0^\pi d\theta \int_0^{2\pi} d\phi \; \sin\theta}
$$
$$
\langle A_\perp \rangle = \frac{\int_0^\pi d\theta \int_0^{2\pi} d\phi \int_0^{2\pi} d\chi \; A_\perp(\theta, \phi, \chi)\sin\theta}{\int_0^\pi d\theta \int_0^{2\pi} d\phi \int_0^{2\pi} d\chi \; \sin\theta}
$$

$$(41)$$

to obtain,

$$
A_\parallel^{\mathrm{GSB}} = -\frac{8}{15}\lambda^2 \tilde{\lambda}^2 |\mu|^4
$$
$$
A_\perp^{\mathrm{GSB}} = -\frac{2}{5}\lambda^2 \tilde{\lambda}^2 |\mu|^4
$$

$$(42)$$

which, using the ground-state bleaching form of Equation 13, gives an anisotropy of

$$
r^{\mathrm{GSB}} = \frac{A_\parallel^{\mathrm{GSB}} - A_\perp^{\mathrm{GSB}}}{A_\parallel^{\mathrm{GSB}} + 2A_\perp^{\mathrm{GSB}}} = 0.1 \; . \qquad (43)
$$

In the following subsections we investigate the absorption from stimulated emission and resulting anisotropy for a circular oscillator with different types of environmental perturbations. These perturbations are decoherence; introduction of an energy gap; and both of these environmental effects together.

A.1   Circularly Degenerate Oscillator Undergoing Decoherence

An arbitrary 2×2 density matrix ρ can be made from a linear combination of Pauli matrices

$$\rho(t) = \frac{\mathbb{I} + \alpha_x(t)X + \alpha_y(t)Y + \alpha_z(t)Z}{2} \tag{44}$$

where X, Y and Z are the Pauli matrices

$$X = \begin{pmatrix} 0 & 1 \\ 1 & 0 \end{pmatrix} \qquad Y = \begin{pmatrix} 0 & -i \\ i & 0 \end{pmatrix} \qquad Z = \begin{pmatrix} 1 & 0 \\ 0 & -1 \end{pmatrix}. \tag{45}$$

Assuming that ρ is written in the eigenbasis, for some arbitrary propagator $U(t) = e^{-iE_x t/\hbar}\,|x\rangle\,\langle x| + e^{-iE_y t/\hbar}\,|y\rangle\,\langle y|$ we have

$$\begin{aligned}
\rho(t) &= U(t) \cdot \rho(0) \cdot U^\dagger(t) \\
&= \frac{\mathbb{I} + \alpha_x(t)X + \alpha_y(t)Y + \alpha_z(0)Z}{2} \\
&= \frac{1}{2}\Bigg(\mathbb{I} + \alpha_x(0)\left[\cos\left(\frac{[E_x - E_y]t}{\hbar} \right) X - \sin\left(\frac{[E_x - E_y]t}{\hbar} \right) Y \right] \\
&\quad + \alpha_y(0)\left[\sin\left(\frac{[E_x - E_y]t}{\hbar} \right) X + \cos\left(\frac{[E_x - E_y]t}{\hbar} \right) Y \right] + \alpha_z(0)Z \Bigg) \\
&= \frac{\mathbb{I} + |\alpha_{xy}(0)|\left[\cos\left(\frac{(E_x - E_y)t}{\hbar} + \xi \right) X + \sin\left(\frac{(E_x - E_y)t}{\hbar} + \xi \right) Y \right] + \alpha_z(0)Z}{2}
\end{aligned} \tag{46}$$

where $\alpha_x(0) = |\alpha_{xy}(0)| \cos(\xi)$ and $\alpha_y(0) = |\alpha_{xy}(0)| \sin(\xi)$, so ξ is the phase of the coherence in the initial density matrix.

Dephasing is the process by which the magnitude of the off-diagonal elements (given by $|\alpha_{xy}|$) decays to 0; we will use γ to denote the rate of this process. We can use the relationships that $Z \cdot X \cdot Z = -X$, $Y \cdot Z \cdot Y = -Y$ and $Z \cdot Z \cdot Z = Z$ to show that $Z \cdot \rho(t) \cdot Z = (\mathbb{I} - \alpha_x(t)X - \alpha_y(t)Y + \alpha_z(t)Z)/2$. Using this we can define $\mathcal{L}_{\text{dephase}}(\rho, t)$ the action of the Lindblad superoperator which dephases the density matrix and propagates it

through a time t

$$
\begin{aligned}
\mathcal{L}_{\text{dephase}}(\rho(0), t) &= \frac{\rho(t)(1 + e^{-\gamma t}) + Z \cdot \rho(t) \cdot Z(1 - e^{-\gamma t})}{2} \\
&= \frac{\mathbb{I} + e^{-\gamma t}\alpha_x(t)X + e^{-\gamma t}\alpha_y(t)Y + \alpha_z(0)Z}{2} \\
&= \frac{\mathbb{I} + e^{-\gamma t}|\alpha_{xy}(0)|\left[\cos\left(\frac{(E_x - E_y)t}{\hbar} + \xi\right)X + \sin\left(\frac{(E_x - E_y)t}{\hbar} + \xi\right)Y\right] + \alpha_z(0)Z}{2}
\end{aligned}
\tag{47}
$$

These steps rely on the fact that $[H, Z] = 0$.

A similar argument can be made to form a population exchange superoperator. Population exchange has the effect of reducing the density matrix to $\mathbb{I}/2$; this means that $|\alpha_{xy}|$ and $|\alpha_z|$ must decrease. The action of the population-exchange superoperator is thus

$$
\begin{aligned}
\mathcal{L}_{\text{pop}}(\rho(0), t) &= \frac{\rho(t)(1 + 3e^{-2\Gamma t}) + (X \cdot \rho(t) \cdot X + Y \cdot \rho(t) \cdot Y + Z \cdot \rho(t) \cdot Z)(1 - e^{-2\Gamma t})}{4} \\
&= \frac{\mathbb{I} + \alpha_x(t)e^{-2\Gamma t}X + \alpha_y(t)e^{-2\Gamma t}Y + \alpha_z(0)e^{-2\Gamma t}Z}{2} \\
&= \frac{\mathbb{I} + e^{-2\Gamma t}|\alpha_{xy}(0)|\left[\cos\left(\frac{(E_x - E_y)t}{\hbar} + \xi\right)X + \sin\left(\frac{(E_x - E_y)t}{\hbar} + \xi\right)Y\right] + e^{-2\Gamma t}\alpha_z(0)Z}{2},
\end{aligned}
\tag{48}
$$

which reduces the density matrix to $\mathbb{I}/2$ with a rate of 2Γ (this definition of the rate is chosen to match references 48 and 49). Decoherence acts as the combination of the above two processes and has the effect on the density matrix of

$$
\begin{aligned}
\mathcal{L}_{\text{decoh}}(\rho(0), t) &= \frac{\mathbb{I} + \alpha_x(t)e^{-(\gamma + 2\Gamma)t}X + \alpha_y(t)e^{-(\gamma + 2\Gamma)t}Y + \alpha_z(t)e^{-2\Gamma t}Z}{2} \\
&= \frac{\mathbb{I} + e^{-(\gamma + 2\Gamma)t}|\alpha_{xy}(0)|\left[\cos\left(\frac{(E_x - E_y)t}{\hbar} + \xi\right)X + \sin\left(\frac{(E_x - E_y)t}{\hbar} + \xi\right)Y\right] + e^{-2\Gamma t}\alpha_z(0)Z}{2}.
\end{aligned}
\tag{49}
$$

The superoperator $\mathcal{L}_{\text{decoh}}$ is independent of the order of the dephasing and population-exchange processes.

We have now defined the action of decoherence on a 2×2 density matrix. However, the

circular oscillator is a three-level system in the basis of $|\Phi^{(0)}\rangle$, $|x\rangle$ and $|y\rangle$, and we now define the Pauli matrices as

$$
\mathbb{I}_2 = \begin{pmatrix} 0 & 0 & 0 \\ 0 & 1 & 0 \\ 0 & 0 & 1 \end{pmatrix} \qquad X_3 = \begin{pmatrix} 0 & 0 & 0 \\ 0 & 0 & 1 \\ 0 & 1 & 0 \end{pmatrix} \qquad Y_3 = \begin{pmatrix} 0 & 0 & 0 \\ 0 & 0 & -i \\ 0 & i & 0 \end{pmatrix} \qquad Z_3 = \begin{pmatrix} 0 & 0 & 0 \\ 0 & 1 & 0 \\ 0 & 0 & -1 \end{pmatrix}.
$$
(50)

The density matrix at time t after the pulse is

$$
\begin{aligned}
\rho(t) = {} & |c_0|^2 \, |\Phi^{(0)}\rangle \, \langle\Phi^{(0)}| + \left[c_0 \sqrt{1-|c_0|^2} \, |v(t)\rangle \, \langle\Phi^{(0)}| + c_0^* \sqrt{1-|c_0|^2} \, |\Phi^{(0)}\rangle \, \langle v(t)| \right] \\
& + \frac{1}{2}(1-|c_0|^2)\left(\mathbb{I}_2 + e^{-2\Gamma t}\alpha_z(0) Z_3 \right. \\
& \left. + e^{-(\gamma+2\Gamma)t}|\alpha_{xy}(0)| \left[\cos\left(\frac{(E_x - E_y)t}{\hbar} + \xi \right) X_3 + \sin\left(\frac{(E_x - E_y)t}{\hbar} + \xi \right) Y_3 \right] \right),
\end{aligned}
$$
(51)

where $|v(t)\rangle$ is some complicated but computable state, spanning the space of $|x\rangle$ and $|y\rangle$, which can become un-normalised through decoherence. The absorption does not depend on $|v(t)\rangle$ so we do not describe it here, although we have however given all the details needed to calculate it. The constants above have the values of $(1-|c_0|^2) = \lambda\mu(\varepsilon_x^2 + \varepsilon_y^2)$ and $\alpha_z(0) = (\varepsilon_x^2 - \varepsilon_y^2)/(\varepsilon_x^2 + \varepsilon_y^2)$. As the excitation is initially coherent $\alpha_{xy}(0)^2 = 1 - \alpha_z(0)^2$. The phase $\xi = 0$ if $\varepsilon_x\varepsilon_y$ is positive and $\xi = \pi$ if $\varepsilon_x\varepsilon_y$ is negative.

For the case of a circularly degenerate oscillator $E_x - E_y = 0$, which simplifies Equation 51. With the above definitions of R (Equation 37) and $\tilde{R}$ (Equation 38), we can calculate the stimulated-emission absorption using Equation 36:

$$
A^{\mathrm{SE}} = -\frac{\lambda^2\tilde{\lambda}^2|\mu|^4}{2}\left((\varepsilon_x^2 + \varepsilon_y^2)(\tilde{\varepsilon}_x^2 + \tilde{\varepsilon}_y^2) + e^{-2\Gamma t}(\varepsilon_x^2 - \varepsilon_y^2)(\tilde{\varepsilon}_x^2 - \tilde{\varepsilon}_y^2) + 4e^{-(\gamma+2\Gamma)t}\varepsilon_x\tilde{\varepsilon}_x\varepsilon_y\tilde{\varepsilon}_y \right)
$$
(52)

which with orientational averaging becomes

$$
\begin{aligned}
A_\parallel^{\mathrm{SE}} &= -\frac{2}{15}\left(2 + e^{-2\Gamma t} + e^{-t(\gamma+2\Gamma)}\right)\lambda^2\tilde{\lambda}^2|\mu|^4 \\
A_\perp^{\mathrm{SE}} &= -\frac{1}{15}\left(3 - e^{-2\Gamma t} - e^{-t(\gamma+2\Gamma)}\right)\lambda^2\tilde{\lambda}^2|\mu|^4
\end{aligned}
\tag{53}
$$

which using a slightly modified groundstate bleaching version of Equation 13 gives

$$
\begin{aligned}
r^{\mathrm{SE}} &= \frac{A_\parallel^{\mathrm{SE}} - A_\perp^{\mathrm{SE}}}{A_\parallel^{\mathrm{SE}} + 2A_\perp^{\mathrm{SE}}} \\
&= \frac{1}{10}(1 + 3e^{-2\Gamma t} + 3e^{-(\gamma+2\Gamma)t}) ,
\end{aligned}
\tag{54}
$$

and agrees exactly with Naqvi $et\ al.$,[48] and only differs from Wynne $et\ al.$[49] due to our (and reference 48's) definition of population exchange. All three works agree that at very short time scale $r^{\mathrm{SE}} = 0.7$, in the medium time limit when $\gamma^{-1} \ll t \ll \Gamma^{-1}$ then $r^{\mathrm{SE}} = 0.4$, and in the long time limit of $r^{\mathrm{SE}} = 0.1$. When the contribution from with A^{GSB} is included, we obtain

$$
\begin{aligned}
r &= \frac{(A_\parallel^{\mathrm{GSB}} + A_\parallel^{\mathrm{SE}}) - (A_\perp^{\mathrm{GSB}} + A_\perp^{\mathrm{SE}})}{(A_\parallel^{\mathrm{GSB}} + A_\parallel^{\mathrm{SE}}) + 2(A_\perp^{\mathrm{GSB}} + A_\perp^{\mathrm{SE}})} \\
&= \frac{1}{10}(1 + e^{-2\Gamma t} + e^{-(\gamma+2\Gamma)t})
\end{aligned}
\tag{55}
$$

for the full anisotropy.

A.2 Perturbed Circular Without Decoherence

We consider a perturbed circular oscillator in which there is an energy difference between the two states $|x\rangle$ and $|y\rangle$. Taking Equation 51 with $e^{-\gamma t} = 1$ and $e^{-2\Gamma t} = 1$ for all t, and then using Equation 36 gives

$$
A^{\mathrm{SE}} = -\left[\varepsilon_x^2\tilde{\varepsilon}_x^2 + \varepsilon_y^2\tilde{\varepsilon}_y^2 + 2\varepsilon_x\tilde{\varepsilon}_x\varepsilon_y\tilde{\varepsilon}_y\cos\left(\frac{E_x - E_y}{\hbar}t\right)\right]\lambda^2\tilde{\lambda}^2|\mu|^4
\tag{56}
$$

(using the fact that the energies are real values). Performing the same orientational averaging as above gives absorptions

$$A_\parallel^{\text{SE}} = -\frac{2}{15}\left(3 + \cos(\frac{E_x - E_y}{\hbar}t)\right)\lambda^2\tilde{\lambda}^2|\mu|^4$$

$$A_\perp^{\text{SE}} = -\frac{1}{15}\left(2 - \cos(\frac{E_x - E_y}{\hbar}t)\right)\lambda^2\tilde{\lambda}^2|\mu|^4 \tag{57}$$

and anisotropies

$$r^{\text{SE}} = \frac{1}{10}\left(4 + 3\cos(\frac{E_x - E_y}{\hbar}t)\right)$$

$$r = \frac{1}{10}\left(2 + \cos(\frac{E_x - E_y}{\hbar}t)\right) \tag{58}$$

which all agree with reference 68.

A.3   Perturbed Circular Oscillator Undergoing Decoherence

Evaluating Equation 51 for the stimulated emission absorption now yields

$$A^{\text{SE}} = -\frac{\lambda^2\tilde{\lambda}^2|\mu|^4}{2}\Big[(\varepsilon_x^2 + \varepsilon_y^2)(\tilde{\varepsilon}_x^2 + \tilde{\varepsilon}_y^2) + (\varepsilon_x^2 - \varepsilon_y^2)(\tilde{\varepsilon}_x^2 - \tilde{\varepsilon}_y^2)e^{-2\Gamma t}$$
$$+ 4\varepsilon_x\varepsilon_y\tilde{\varepsilon}_x\tilde{\varepsilon}_y e^{-(\gamma+2\Gamma)t}\cos\left(\frac{E_x - E_y}{\hbar}t\right)\Big] , \tag{59}$$

which with orientational averaging becomes

$$A_\parallel^{\text{SE}} = -\frac{2}{15}\left[2 + e^{-2t\Gamma} + e^{-2(\gamma+\Gamma)t}\cos\left(\frac{E_x - E_y}{\hbar}t\right)\right]\lambda^2\tilde{\lambda}^2|\mu|^4$$

$$A_\perp^{\text{SE}} = -\frac{1}{15}\left[3 - e^{-2t\Gamma} - e^{-2(\gamma+\Gamma)t}\cos\left(\frac{E_x - E_y}{\hbar}t\right)\right]\lambda^2\tilde{\lambda}^2|\mu|^4 , \tag{60}$$

and gives anisotropies

$$r^{\text{SE}} = \frac{1}{10}\left(1 + 3e^{-2\Gamma t} + 3e^{-(\gamma+2\Gamma)t}\cos(\frac{E_x - E_y}{\hbar}t)\right)$$

$$r = \frac{1}{10}\left(1 + e^{-2\Gamma t} + e^{-(\gamma+2\Gamma)t}\cos(\frac{E_x - E_y}{\hbar}t)\right) . \tag{61}$$

We are not aware of these equations having appeared in previous work.

B   Absorbtion Ratios

The total absorption difference is given by $\Delta A = A^{\text{GSB}} + A^{\text{SE}}$. We wish to investigate how the relative magnitudes of these two terms change with the number of states coupling to the radiation field. A state can be thought of as coupling to the field if $\delta_k \not\ll \delta_J$, where J is the state with the strongest coupling. Let us now define a system where the coupling is binary and the value of any δ_k is either 0 or δ. We have M $(\tilde{M})$ of the m values of δ_k $(\tilde{\delta_k})$ being non zero, and $m - M$ $(m - \tilde{M})$ being zero.

The value of A^{GSB} is time independent and given in Equation 29 as $-\sum_k^m |\delta_k|^2 \sum_k^m |\tilde{\delta_k}|^2$. For the system described above this has the value $A^{\text{GSB}} = -M\tilde{M}\delta^2\tilde{\delta}^2$, which in quadratic is the number of coupling states.

The stimulated emission signal $A^{\text{SE}}(t)$ is time dependent, and therefore must be time averaged. Let us define the long time average as

$$\langle f(t) \rangle_T := \frac{1}{T} \int_0^T f(t)\, dt \ . \tag{62}$$

The function e^{ixt} will later be shown to be important, we calculate its long time average as

$$\langle e^{ixt} \rangle_T := \begin{cases} \frac{1}{T}\left(\frac{e^{ixT}-1}{ix}\right) \to 0 \text{ as } T \to \infty & \text{if } x \neq 0 \\ \langle 1 \rangle_T = 1 & \text{if } x = 0 \end{cases} \ . \tag{63}$$

The stimulated emission absorption is given in Equation 29c as $A^{\text{SE}}(t) = -\left| \sum_k^m \tilde{\delta}_k^* \delta_k e^{-iE_k t/\hbar} \right|^2$,

simplifying by using the notation $\omega_k = E_k/\hbar$, and setting $\alpha_k = \tilde{\delta}_k^* \delta_k$ we obtain

$$
\begin{aligned}
\langle A^{\text{SE}}(t) \rangle_T &= \frac{1}{T} \int_0^T -\left| \sum_k^m \alpha_k e^{-i\omega_k t} \right|^2 dt \\
&= \frac{1}{T} \int_{t'}^{\infty} -\sum_k^m |\alpha_k|^2 - \sum_{k' \neq k}^m \alpha_k \alpha_{k'}^* e^{i(\omega_{k'} - \omega_k)t} \ dt
\end{aligned}
\tag{64}
$$

which using Equation 63 gives

$$
\langle A^{\text{SE}}(t) \rangle_T = \sum_k^m |\alpha_k|^2 = \sum_k^m |\delta_k|^2 |\tilde{\delta}_k|^2 \ ,
\tag{65}
$$

under the condition that no two states are degenerate. When the above expression is evaluated for our model system, the maximum value of $\langle A^{\text{SE}}(t) \rangle_T$ is bounded by either $M\delta\tilde{\delta}$ or $\tilde{M}\delta\tilde{\delta}$ depending on which is stricter.

We can also calculate the average variations in $A^{SE}(t)$ in the long time limit by evaluating the standard deviation $\sigma[A^{\text{SE}}(t)]$

$$
\begin{aligned}
\sigma[A^{\text{SE}}(t)]^2 &= \frac{1}{T} \int_0^T \left[\left| \sum_k \alpha_k e^{-i\omega_k t} \right|^2 - \sum_k |\alpha_k|^2 \right]^2 dt \\
&= \frac{1}{T} \int_0^T \left[\sum_{k \neq k'} \alpha_k \alpha_{k'}^* e^{-i(\omega_k - \omega_{k'})t} \right]^2 dt \\
&= \frac{1}{T} \int_0^T \left[\sum_{k \neq k'} \sum_{j \neq j'} \alpha_k \alpha_{k'}^* \alpha_{j'} \alpha_j^* e^{-i(\omega_k - \omega_{k'} + \omega_j - \omega_{j'})t} \right]^2 dt
\end{aligned}
\tag{66}
$$

which using Equation 63 gives

$$
\begin{aligned}
\sigma[A^{\text{SE}}(t)]^2 &= \sum_{k \neq k'} |\alpha_k \alpha_{k'}|^2 \\
\sigma[A^{\text{SE}}(t)] &= \sqrt{\sum_{k \neq k'}^m (\alpha_k \alpha_{k'}^*)^2}
\end{aligned}
\tag{67}
$$

under the condition that there are no degeneracies in the gaps between energy levels. The value of $\sigma[A^{\text{SE}}(t)]$ for our model system is bounded by the smaller of $M\delta\tilde{\delta}$ and $\tilde{M}\delta\tilde{\delta}$.

We have therefore shown that if M or $\tilde{M}$ is large (particularly when M and $\tilde{M}$ are very different) the total absorption is dominated by the ground-state bleaching term. This means the anisotropy tends to that of the ground-state bleaching which is 0.1.

References

(1) Sauer, K. Photosynthesis: The Light Reactions. *Annu. Rev. Phys. Chem.* **1979**, *30*, 155–78.

(2) van der Weij-De Wit, C. D.; Doust, A. B.; Van Stokkum, I. H. M.; Dekker, J. P.; Wilk, K. E.; Curmi, P. M. G.; Scholes, G. D.; van Grondelle, R. How Energy Funnels from the Phycoerythrin Antenna Complex to Photosystem I and Photosystem II in Cryptophyte Rhodomonas CS24 Cells. *J. Phys. Chem. B* **2006**, *110*, 25066–25073.

(3) Scholes, G. D. Quantum-Coherent Electronic Energy Transfer: Did Nature Think of it First? *J. Phys. Chem. Lett.* **2010**, *1*, 2–8.

(4) Scholes, G. D.; Fleming, G. R.; Olaya-Castro, A.; van Grondelle, R. Lessons from Nature About Solar Light Harvesting. *Nat. Chem.* **2011**, *3*, 763–774.

(5) Brixner, T.; Stenger, J.; Vaswani, H. M.; Cho, M.; Blankenship, R. E.; Fleming, G. R. Two-Dimensional Spectroscopy of Electronic Couplings in Photosynthesis. *Nature* **2005**, *434*, 625–628.

(6) Lee, H.; Cheng, Y.-C.; Fleming, G. R. Coherence Dynamics in Photosynthesis: Protein Protection of Excitonic Coherence. *Science* **2007**, *316*, 1462–1465.

(7) Engel, G. S.; Calhoun, T. R.; Read, E. L.; Ahn, T.-K.; Mancal, T.; Cheng, Y.-C.; Blankenship, R. E.; Fleming, G. R. Evidence for Wavelike Energy Transfer Through Quantum Coherence in Photosynthetic Systems. *Nature* **2007**, *446*, 782–786.

(8) Collini, E.; Wong, C. Y.; Wilk, K. E.; Curmi, P. M. G.; Brumer, P.; Scholes, G. D. Coherently Wired Light-Harvesting in Photosynthetic Marine Algae at Ambient Temperature. *Nature* **2010**, *463*, 644–647.

(9) Panitchayangkoon, G.; Hayes, D.; Fransted, K. A.; Caram, J. R.; Harel, E.; Wen, J.; Blankenship, R. E.; Engel, G. S. Long-Lived Quantum Coherence in Photosynthetic Complexes at Physiological Temperature. *Proc. Natl. Acad. Sci.* **2010**, *107*, 12766–12770.

(10) Harel, E.; Engel, G. S. Quantum Coherence Spectroscopy Reveals Complex Dynamics in Bacterial Light-Harvesting Complex 2 (LHII). *Proc. Natl. Acad. Sci.* **2012**, *109*, 706–711.

(11) Calhoun, T. R.; Ginsberg, N. S.; Schlau-Cohen, G. S.; Cheng, Y.-C.; Ballottari, M.; Bassi, R.; Fleming, G. R. Quantum Coherence Enabled Determination of the Energy Landscape in Light Harvesting Complex II. *J Phys Chem B* **2009**, *113*, 16291–16295.

(12) Fuller, F. D.; Pan, J.; Gelzinis, A.; Butkus, V.; Senlik, S. S.; Wilcox, D. E.; Yocum, C. F.; Valkunas, L.; Abramavicius, D.; Ogilvie, J. P. Vibronic Coherence in Oxygenic Photosynthesis. *Nat. Chem.* **2014**, *6*, 706–11.

(13) Romero, E.; Augulis, R.; Novoderezhkin, V. I.; Ferretti, M.; Thieme, J.; Zigmantas, D.; van Grondelle, R. Quantum Coherence in Photosynthesis for Efficient Solar-Energy Conversion. *Nat. Phys.* **2014**, *10*, 676–682.

(14) Sension, R. J. Biophysics: Quantum Path to Photosynthesis. *Nature* **2007**, *446*, 740–741.

(15) Plenio, M. B.; Huelga, S. F. Dephasing-Assisted Transport: Quantum Networks and Biomolecules. *New J. Phys.* **2008**, *10*, 113019.

(16) León-Montiel, R. J.; Torres, J. P. Highly Efficient Noise-Assisted Energy Transport in Classical Oscillator Systems. *Phys. Rev. Lett.* **2013**, *110*, 218101.

(17) Sato, Y.; Doolittle, B. Influence of Intra-Pigment Vibrations on Dynamics of Photosynthetic Exciton. *J. Chem. Phys.* **2014**, *141*, 185102.

(18) Forgy, C. C.; Mazziotti, D. A. Relations Between Environmental Noise and Electronic Coupling for Optimal Exciton Transfer in One- and Two-Dimensional Homogeneous and Inhomogeneous Quantum Systems. *J. Chem. Phys.* **2014**, *141*, 224111.

(19) Caruso, F.; Chin, a. W.; Datta, A.; Huelga, S. F.; Plenio, M. B. Highly Efficient Energy Excitation Transfer in Light-Harvesting Complexes: The Fundamental Role of Noise-Assisted Transport. *J. Chem. Phys.* **2009**, *131*.

(20) Nalbach, P.; Mujica-Martinez, C. a.; Thorwart, M. Vibronic Speed-Up of the Excitation Energy Transfer in the Fenna-Matthews-Olson Complex. *Phys. Rev. E* **2013**, *91*, 022706.

(21) Christensson, N.; Kauffmann, H. F.; Pullerits, T.; Mančal, T. Origin of Long-Lived Coherences in Light-Harvesting Complexes. *J. Phys. Chem. B* **2012**, *116*, 7449–7454.

(22) Tiwari, V.; Peters, W. K.; Jonas, D. M. Electronic Resonance with Anticorrelated Pigment Vibrations Drives Photosynthetic Energy Transfer Outside the Adiabatic Framework. *Proc. Natl. Acad. Sci.* **2013**, *110*, 1203–1208.

(23) Fujihashi, Y.; Fleming, G. R.; Ishizaki, A. Impact of Environmentally Induced Fluctuations on Quantum Mechanically Mixed Electronic and Vibrational Pigment States in Photosynthetic Energy Transfer and 2D Electronic Spectra. *J. Chem. Phys.* **2015**, *142*, 212403.

(24) Lim, J.; Palecek, D.; Caycedo-soler, F.; Lincoln, C. N.; Prior, J.; Berlepsch, H. V.

Verification of the Vibronic Origin of Long-Lived Coherence in an Artificial Molecular Light Harvester. *Nat. Commun.* **2015**, *6*, 7755.

(25) Monahan, D. M.; Whaley-Mayda, L.; Ishizaki, A.; Fleming, G. R. Influence of Weak Vibrational-Electronic Couplings on 2D Electronic Spectra and Inter-Site Coherence in Weakly Coupled Photosynthetic Complexes. *J. Chem. Phys.* **2015**, *143*, 065101.

(26) Cho, M.; Vaswani, H. M.; Brixner, T.; Stenger, J.; Fleming, G. R. Exciton Analysis in 2D Electronic Spectroscopy. *J. Phys. Chem. B* **2005**, *109*, 10542–56.

(27) Redfield, A. On the Theory of Relaxation Processes. *IBM J. Res. Dev.* **1957**, *1*, 19–31.

(28) Jang, S. Generalization of the Förster Resonance Energy Transfer Theory for Quantum Mechanical Modulation of the Donor-Acceptor Coupling. *J. Chem. Phys.* **2007**, *127*, 174710.

(29) Jang, S.; Jung, Y.; Silbey, R. J. Nonequilibrium Generalization of Förster-Dexter Theory for Excitation Energy Transfer. *Chem. Phys.* **2002**, *275*, 319–332.

(30) Jang, S.; Newton, M. D.; Silbey, R. J. Multichromophoric Förster Resonance Energy Transfer. *Phys. Rev. Lett.* **2004**, *92*, 218301.

(31) Ishizaki, A.; Fleming, G. R. Theoretical Examination of Quantum Coherence in a Photosynthetic System at Physiological Temperature. *Proc. Natl. Acad. Sci.* **2009**, *106*, 17255–17260.

(32) Hwang-Fu, Y.-H.; Chen, W.; Cheng, Y.-C. A Coherent Modified Redfield Theory for Excitation Energy Transfer in Molecular Aggregates. *Chem. Phys.* **2014**, *447*, 46–53.

(33) Lindblad, G. On the Generators of Quantum Dynamical Semigroups. *Commun. Math. Phys.* **1976**, *48*, 1976.

(34) Cogdell, R. J.; Gall, A.; Köhler, J. The Architecture and Function of the Light-Harvesting Apparatus of Purple Bacteria: From Single Molecules to in Vivo Membranes. *Q. Rev. Biophys.* **2006**, *39*, 227–324.

(35) Cleary, L.; Chen, H.; Chuang, C.; Silbey, R. J.; Cao, J. Optimal Fold Symmetry of LH2 Rings on a Photosynthetic Membrane. *Proc. Natl. Acad. Sci.* **2013**, *101*.

(36) McDermott, G.; Cogdell, R. J. Crystal Structure of an Integral Membrane Light-Harvesting Complex from Photosynthetic Bacteria. *Nature* **1995**, *374*, 517–521.

(37) Kennis, J. T. M.; Streltsov, A. M.; Vulto, S. I. E.; Aartsma, T. J.; Nozawa, T.; Amesz, J. Femtosecond Dynamics in Isolated LH2 Complexes of Various Species of Purple Bacteria. *J. Phys. Chem. B* **1997**, *101*, 7827–7834.

(38) Jimenez, R.; Dikshit, S.; Bradforth, S. E.; Fleming, G. R. Electronic Excitation Transfer in the LH2 Complex of Rhodobacter Sphaeroides. *J. Phys. Chem.* **1996**, *100*, 6825–6834.

(39) Nagarajan, V.; Alden, R. Ultrafast Exciton Relaxation in the B850 Antenna Complex of Rhodobacter sphaeroides. *Proc. Natl. Acad. Sci.* **1996**, *93*, 13774–13779.

(40) Nagarajan, V.; Johnson, E. T.; Williams, J. C.; Parson, W. W. Femtosecond Pump-Probe Spectroscopy of the B850 Antenna Complex of Rhodobacter sphaeroides at Room Temperature. *J. Phys. Chem. B* **1999**, *103*, 2297–2309.

(41) Vulto, S. I. E.; Kennis, J. T. M.; Streltsov, A. M.; Amesz, J.; Aartsma, T. J. Energy Relaxation within the B850 Absorption Band of the Isolated Light-Harvesting Complex LH2 from Rhodopseudomonas acidophila at Low Temperature. *J. Phys. Chem. B* **1999**, *103*, 878–883.

(42) Book, L. D.; Ostafin, a. E.; Ponomarenko, N.; Norris, J. R.; Scherer, N. F. Exciton

Delocalization and Initial Dephasing Dynamics of Purple Bacterial LH2. *J. Phys. Chem. B* **2000**, *104*, 8295–8307.

(43) Book, L. D.; Ostafin, A. E.; Ponomarenko, N.; Norris, J. R.; Mukamel, S.; Scherer, N. F. Time-Dependent Exciton Delocalization Size in the B850 Band of Purple Bacterial LH2. Ultrafast Phenom. Xii. 2000; pp 659–661.

(44) Chachisvilis, M.; Kühn, O.; Pullerits, T.; Sundström, V. Excitons in Photosynthetic Purple Bacteria: Wavelike Motion or Incoherent Hopping? *J. Phys. Chem. B* **1997**, *101*, 7275–7283.

(45) Pullerits, T.; Chachisvilis, M.; Sundström, V. Exciton Delocalization Length in the B850 Antenna of Rhodobacter Sphaeroides. *J. Phys. Chem.* **1996**, *100*, 10787–10792.

(46) Galli, C.; Wynne, K.; LeCours, S. M.; Therien, M.; Hochstrasser, R. Direct Measurement of Electronic Dephasing using Anisotropy. *Chem. Phys. Lett.* **1993**, *206*, 493–499.

(47) Kühn, O.; Sundström, V. Pump-Probe Spectroscopy of Dissipative Energy Transfer Dynamics in Photosynthetic Antenna Complexes: A Density Matrix Approach. *J. Chem. Phys.* **1997**, *107*, 4154–4164.

(48) Naqvi, K. R.; Dale, R. E. Ultrafast Decay of Anisotropy Due to Electronic Decoherence in Systems with Twofold or Threefold Degeneracy. *Chem. Phys. Lett.* **2002**, *357*, 147–152.

(49) Wynne, K.; Hochstrasser, R. M. Coherence Effects in the Anisotropy of Optical Experiments. *Chem. Phys.* **1993**, *171*, 179–188.

(50) Frenkel, J. On the Transformation of Light into Heat in Solids. I. *Phys. Rev.* **1931**, *37*, 17–44.

(51) Stone, A. J. *The Theory of Intermolecular Forces*; Clarendon Press, 1997.

(52) Damjanovič, A.; Kosztin, I.; Kleinekathöfer, U.; Schulten, K. Excitons in a Photosynthetic Light-Harvesting System: A Combined Molecular Dynamics, Quantum Chemistry, and Polaron Model Study. *Phys. Rev. E* **2002**, *65*, 031919.

(53) Steinmann, C.; Kongsted, J. Electronic Energy Transfer in Polarizable Heterogeneous Environments: A Systematic Investigation of Different Quantum Chemical Approaches. *J. Chem. Theory Comput.* **2015**, *11*, 4283–4293.

(54) Neugebauer, J. Photophysical Properties of Natural Light-Harvesting Complexes Studied by Subsystem Density Functional Theory. *J. Phys. Chem. B* **2008**, *112*, 2207–2217.

(55) König, C.; Neugebauer, J. Protein Effects on the Optical Spectrum of the Fenna-Matthews-Olson Complex From Fully Quantum Chemical Calculations. *J. Chem. Theory Comput.* **2013**, *9*, 1808–1820.

(56) Kenny, E. P.; Kassal, I. Benchmarking Calculations of Excitonic Couplings Between Bacteriochlorophylls. **2015**, 1–8.

(57) University of Karlsruhe, TURBOMOLE V6.4 2012. 2007; http://www.turbomole.com.

(58) Stephens, P. J.; Devlin, F. J.; Chabalowski, C. F.; Frisch, M. J. Ab Initio Calculation of Vibrational Absorption and Circular Dichroism Spectra Using Density Functional Force Fields. *J. Phys. Chem.* **1994**, *98*, 11623–11627.

(59) Adamo, C.; Barone, V. Toward Reliable Density Functional Methods without Adjustable Parameters: The PBE0 model. *J. Chem. Phys.* **1999**, *110*, 6158–6170.

(60) Schäfer, A.; Horn, H.; Ahlrichs, R. Fully Optimized Contracted Gaussian Basis Sets for Atoms Li to Kr. *J. Chem. Phys.* **1992**, *97*, 2571–2577.

(61) Gouterman, M. Spectra of Porphyrins. *J. Mol. Spectrosc.* **1961**, *6*, 138–163.

(62) Krueger, B. P.; Scholes, G. D.; Fleming, G. R. Calculation of Couplings and Energy-Transfer Pathways between the Pigments of LH2 by the ab Initio Transition Density Cube Method. *J. Phys. Chem. B* **1998**, *102*, 5378–5386.

(63) Georgakopoulou, S.; Frese, R. N.; Johnson, E.; Koolhaas, C.; Cogdell, R. J.; van Grondelle, R.; van der Zwan, G. Absorption and CD Spectroscopy and Modelling of Various LH2 Complexes from Purple Bacteria. *Biophys. J.* **2002**, *82*, 2184–2197.

(64) Chuang, I.; Nielsen, M. *Quantum Computation and Quantum Information*; Cambridge University Press, 2000.

(65) Dawlaty, J. M.; Ishizaki, A.; De, A. K.; Fleming, G. R. Microscopic Quantum Coherence in a Photosynthetic-Light-Harvesting Antenna. *Philos. Trans. R. Soc. A Math. Phys. Eng. Sci.* **2012**, *370*, 3672–3691.

(66) Schlosshauer, M. A. *Decoherence: and the Quantum-To-Classical Transition*; 2007.

(67) Ishizaki, A.; Fleming, G. R. On the Interpretation of Quantum Coherent Beats Observed in Two-Dimensional Electronic Spectra of Photosynthetic Light Harvesting Complexes. *J. Phys. Chem. B* **2011**, *115*, 6227–6233.

(68) Savikhin, S.; Buck, D. R.; Struve, W. S. Oscillating Anisotropies in a Bacteriochlorophyll Protein: Evidence for Quantum Beating Between Exciton Levels. *Chem. Phys.* **1997**, *223*, 303–312.

(69) Matsushita, M.; Ketelaars, M.; van Oijen, a. M.; Köhler, J.; Aartsma, T. J.; Schmidt, J. Spectroscopy on the B850 Band of Individual Light-Harvesting 2 Complexes of Rhodopseudomonas Acidophila. II. Exciton States of an Elliptically Deformed Ring Aggregate. *Biophys. J.* **2001**, *80*, 1604–1614.

(70) Bradforth, S. E.; Jimenez, R.; van Mourik, F.; van Grondelle, R.; Fleming, G. R. Excitation Transfer in the Core Light-Harvesting Complex (LH-1) of Rhodobacter

sphaeroides: An Ultrafast Fluorescence Depolarization and Annihilation Study. *J. Phys. Chem.* **1995**, *99*, 16179–16191.

(71) Hofmann, C.; Aartsma, T. J.; Kahler, J. Energetic Disorder and the B850-Exciton States of Individual Light-Harvesting 2 Complexes from Rhodopseudomonas Acidophila. *Chem. Phys. Lett.* **2004**, *395*, 373–378.

(72) Hamm, P.; Zanni, M. *Concepts and Methods of 2D Infrared Spectroscopy*; Cambridge University Press, 2011.

(73) Smith, E. R.; Jonas, D. M. Alignment, Vibronic Level Splitting, and Coherent Coupling Effects on the Pump-Probe Polarization Anisotropy. *J. Phys. Chem. A* **2011**, *115*, 4101–4113.

(74) Jonas, D.; Lang, M.; Nagasawa, Y. Pump-Probe Polarization Anisotropy Study of Femtosecond Energy Transfer within the Photosynthetic Reaction Center of Rhodobacter Sphaeroides R26. *J. Phys. Chem.* **1996**, *3654*, 12660–12673.

(75) van Grondelle, R.; Novoderezhkin, V. I. Energy transfer in photosynthesis: experimental insights and quantitative models. *Phys. Chem. Chem. Phys.* **2006**, *8*, 793–807.

(76) Spano, F. C.; Mukamel, S. Superradiance in Molecular Aggregates. *J. Chem. Phys.* **1989**, *91*, 683–700.

(77) Spano, F. C.; Mukamel, S. Nonlinear Susceptibilities of Molecular Aggregates. *Phys. Rev. A* **1989**, *40*, 5243.

(78) Novoderezhkin, V.; Monshouwer, R.; van Grondelle, R. Exciton (De)localization in the LH2 Antenna of Rhodobacter Sphaeroides as Revealed by Relative Difference Absorption Measurements of the LH2 Antenna and the B820 Subunit. *J. Phys. Chem. A* **1999**, *103*, 10540–10548.

1
2
3
4
5
6
7
8
9
10
11
12
13
14
15
16
17
18
19
20
21
22
23
24
25
26
27
28
29
30
31
32
33
34
35
36
37
38
39
40
41
42
43
44
45
46
47
48
49
50
51
52
53
54
55
56
57
58
59
60